

## MEAN FLOW MEASUREMENTS IN VERY HIGH REYNOLDS NUMBER TURBULENT BOUNDARY LAYER

M. Vallikivi, M. Hultmark and A. J. Smits

Department of Mechanical and Aerospace Engineering  
Princeton University, Princeton, NJ  
mvalliki@princeton.edu

### ABSTRACT

Measurements are presented of the mean flow behavior in zero pressure gradient, flat plate, turbulent boundary layer for Reynolds numbers from  $Re_\theta = 8.8 \times 10^3$  to  $Re_\theta = 225 \times 10^3$ . The measurements were conducted in the High Reynolds number Test Facility (HRTF) at Princeton University which uses compressed air as the working fluid. The mean velocity profiles were measured using Pitot probes as well as Nano-Scale Thermal Anemometry Probes (NSTAPs). The results demonstrate excellent agreement with each other, and support the suggestions made by previous authors that the von Kármán constant for turbulent boundary layers is close to a value of 0.39 and that the logarithmic region extends up to  $y/\delta = 0.15$ .

### INTRODUCTION

The scaling of turbulent wall-bounded flows with Reynolds number has been the subject of considerable interest (see, for example, Marusic *et al.* 2010, and Smits *et al.* 2011). Boundary layers, pipe flows and channel flows are often assumed to scale with the same variables, namely the friction velocity  $u_\tau = \sqrt{\tau_w/\rho}$  and either the viscous length scale  $\nu/u_\tau$  for the inner region of the flow, or the boundary layer thickness  $\delta$  (radius  $R$  for pipes, half height  $h$  for channels) for the outer flow. Here,  $\tau_w$  is the wall shear stress,  $\rho$  is the density of the fluid, and  $\nu$  is its kinematic viscosity.

For sufficiently high Reynolds numbers, one can expect an overlap region between the inner and outer scaling of the flow. In this region, often referred to as the inertial subregion, the mean velocity  $U$  can be expected to behave logarithmically, expressed as

$$U^+ = \frac{1}{\kappa} \log y^+ + B, \quad (1)$$

where  $U^+ = U/u_\tau$  and  $y^+ = yu_\tau/\nu$  are respectively the mean velocity and wall-normal distance scaled with inner coordinates,  $\nu$  is the fluid kinematic viscosity,  $\kappa$  is called the von Kármán constant and  $B$  is the additive constant associated with the logarithmic behavior. In recent years, with advancing measurement techniques and facilities, high quality measurements over a wide range of Reynolds numbers have been reported, with some evidence showing that in different wall-bounded flows the start and extent of the logarithmic region, and the value of the von Kármán constant may vary.

The start of the log-law region was commonly assumed to be located at  $y^+ = yu_\tau/\nu = 30 - 50$ , but recent studies in-

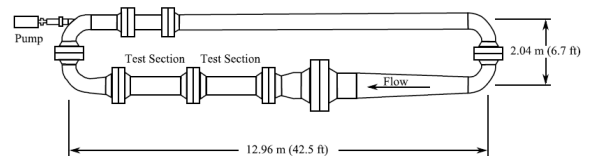


Figure 1. The Princeton High Reynolds Number Test Facility (HRTF).

dicating values as high as  $y^+ = 800$  for pipe flows (Hultmark *et al.* 2012) and for boundary layers, recently a Reynolds number dependent lower limit of  $y^+ = Re_\tau^{0.5}$  has been proposed by Marusic *et al.* (2013), where  $Re_\tau = u_\tau \delta/\nu$ . As to the outer limit, values in the literature range from  $y/\delta = 0.08$  to 0.3, Marusic *et al.* (2013) suggesting  $y/\delta = 0.15$ . The values of the von Kármán constant reported in the past have also varied over a considerable range, with values as low as 0.38 in a boundary layer (Österlund 2000) and as high as 0.42 in a pipe (McKeon *et al.* 2004). More recently, the value of 0.38 given by Nagib & Chauhan (2008) has garnered considerable experimental support, although the maximum Reynolds number  $Re_\tau$  for this data set did not exceed 10,000.

In order to establish these and other parameters more precisely, it is necessary to obtain high quality and high resolution experimental data over a very large range of Reynolds numbers. At Princeton, we have the facilities and the instrumentation to make these measurements possible.

### EXPERIMENT

The boundary layer measurements were conducted in the High Reynolds Number Test Facility (HRTF) at Princeton University Gas Dynamics Laboratory. It is a closed-loop wind tunnel with air as the working fluid that can be compressed up to 220 atm, thus decreasing the kinematic viscosity and therefore allowing to achieve and study a wide range of Reynolds numbers in laboratory conditions. The wind tunnel runs at maximum speed of 12 m/s and has free stream turbulence intensity levels between 0.3 – 0.6%. The tunnel has two working sections, each 2.44 m long with a 0.61 m outer and 0.49 m inner diameter. The sketch of the tunnel is shown in Figure 1 and the tunnel itself has been described in further detail by Jiménez *et al.* (2010).

A 2.06 m flat plate model with an elliptic leading edge

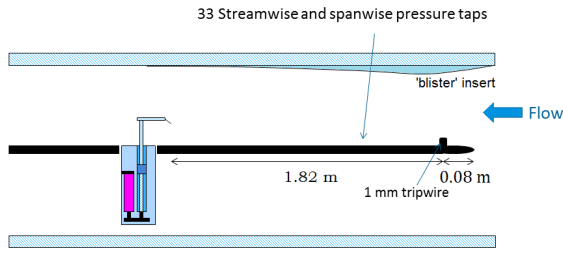


Figure 2. Experimental setup.

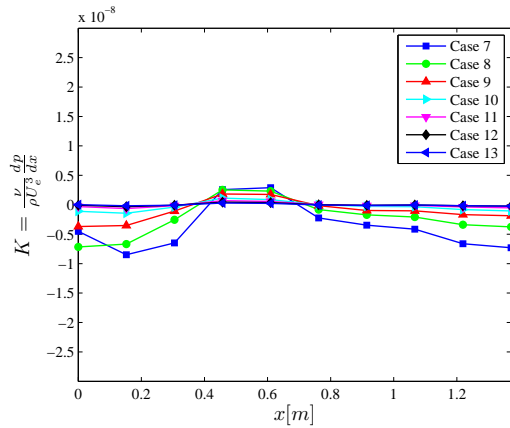


Figure 3. The pressure gradient parameter  $K$ .

was mounted in the downstream test section of the wind tunnel. A 1 mm square trip wire, located at 76 mm from the leading edge, was used to trip the boundary layer and the measurement station was located 1.82 m downstream of the trip wire. The schematic of the setup is shown in Figure 2. The aluminum surface of the plate was carefully polished to a mirror finish. The surface roughness was estimated using an optical microscope and comparator plates and found to be less than  $0.15\mu\text{m}$ , corresponding to  $k_{rms}^+ < 0.4$  at the highest Reynolds number studied. Therefore all experiments reported here pertain to a hydraulically smooth surface.

The pressure distribution in the circular test section was adjusted using a “blister” insert attached to the tunnel wall on the opposite side of the plate, as shown in Figure 2. The pressure distribution was measured using 18 streamwise and 15 spanwise pressure taps and the insert was adjusted to minimize the pressure gradient. The local streamwise pressure gradient parameter (or acceleration parameter)  $K = \frac{\nu}{U_e^3} \frac{dU_e}{dx} = \frac{\nu}{\rho U_e^3} \frac{dp}{dx}$  was found to be always smaller than  $1 \times 10^{-8}$  as shown in Figure 3. This value is at least an order of magnitude smaller than that reported in some previous studies such as the one by DeGraaff & Eaton (2000) where  $K < 1.1 \times 10^{-7}$ , and therefore we can consider the flow to be free of pressure gradient effects.

For the instrumentation, a novel measurement device, a Nano-Scale Thermal Anemometry Probe (NSTAP) was used. The NSTAP has been developed in Princeton in order to resolve small scales of turbulence and allow resolved turbulence measurements at much higher Reynolds numbers

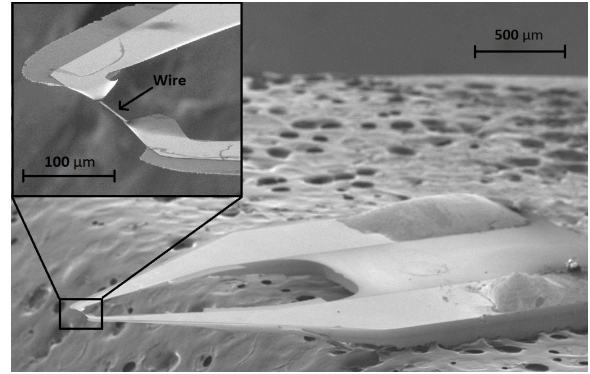


Figure 4. Scanning Electron Microscope image of a Nano-Scale Thermal Anemometry Probe (NSTAP).

than previously possible. These miniature sensors consist of a platinum sensing element and conductive pads supported by an underlying streamlined silicon structure. A representative sensor is shown in Figure 4, with a zoom-in at the front tip of the probe where the sensing element (wire) is located. The NSTAP probes are fabricated using integrated circuit and microelectromechanical systems manufacturing techniques. The fabrication and validation of this novel anemometer are described in Vallikivi *et al.* (2011) and Bailey *et al.* (2010). NSTAPs have been shown to have superior temporal and spatial resolution over conventional hot-wire probes (Hultmark *et al.* 2012).

In the current study, an NSTAP with sensing length of  $\ell = 60\mu\text{m}$  and with  $0.1 \times 2\mu\text{m}$  cross-section was used. The sensor was operated using a Dantec Streamline constant temperature anemometry system with a 1:1 bridge. Probes were calibrated in the freestream against a Pitot tube using 14 calibration points before and after each measurement. The wall-normal distance of the NSTAP probe was measured using a depth measuring microscope and was determined to be  $20\mu\text{m}$  from the wall. At all Reynolds numbers, the initial wall distance was less than 10 viscous units.

In addition to the NSTAP, a Pitot probe was also used to measure the mean velocity profiles. A 0.20 mm diameter Pitot probe in conjunction with two 0.4 mm static pressure taps in the plate was used, and the pressure difference was measured using a DP15 Validyne pressure transducer with a 1.38 kPa range. The transducer was calibrated against a liquid manometer. The wall distance of the Pitot probe was measured using the same optical microscope used for the NSTAP profiles. The Pitot measurements were corrected using the static tap correction (outlined in McKeon *et al.* 2003), viscous and shear corrections following Zagarola & Smits (1998) and the near-wall correction proposed by MacMillan (1956). The data for wall distances smaller than two Pitot tube diameters was neglected in calculations, in order to avoid possible biases introduced by Pitot correction methods and wall distance determination.

Measurements were taken for  $2.6 \times 10^3 < Re^\tau < 65 \times 10^3$ , corresponding to  $8.8 \times 10^3 < Re_\theta < 220 \times 10^3$  where  $Re_\theta = U_e \theta / \nu$  is the Reynolds number based on momentum thickness  $\theta$ . The experimental conditions for all cases are given in Table 1, where  $P$  is the tunnel pressure. The values of  $u_\tau$  given in this table are those derived using the skin friction correlation proposed by Fernholz & Finley (1996).

August 28 - 30, 2013 Poitiers, France

Table 1. Experimental conditions. Cases 1 to 6 were taken using the NSTAP, and Cases 7 to 13 were taken using the Pitot probe. Here,  $Re_\tau = \delta u_\tau / \nu$ .

Case	$Re_\theta$	$Re_\tau$	$P$ [atm]	$U_c$ [m/s]
1	8751	2630	3.50	9.05
2	15,099	4603	7.00	9.34
3	27,464	8318	13.8	9.49
4	48,553	14,601	27.5	9.53
5	85,189	25,520	55.4	9.45
6	139,170	40,665	105	9.50
7	9,447	2866	3.45	9.40
8	16,019	4,848	6.96	9.51
9	28,826	8,726	13.7	9.61
10	50,826	15,312	27.4	9.64
11	91,050	26,777	56.0	9.53
12	148,300	43,786	106	9.58
13	224,800	65,528	213	9.55

## RESULTS

Finding the friction velocity  $u_\tau$  in boundary layers is always a difficult task as there is no easy way to obtain a direct measurement. Most indirect methods are related in one way or another to the presence of a logarithmic layer with known constants, making it difficult to give any conclusive statements about the logarithmic region. In the current study, three different methods were used to estimate the wall shear stress. First, measurements using the 0.2mm Pitot probe as a Preston tube were used to estimate the friction velocity for each Pitot tube test case (Patel 1965, Zagarola *et al.* 2001), and we denote this value by  $u_{\tau P}$ . Second, a Clauser chart technique was used to estimate  $u_{\tau C}$ , where the log law (with  $\kappa = 0.39$  following Marusic *et al.* 2013) was fitted to the velocity profiles for  $y/\delta < 0.15$  (Clauser 1956) for the NSTAP and Pitot tube datasets. Finally, the friction velocity  $u_{\tau F}$  was estimated using the skin friction correlation proposed by Fernholz & Finley (1996) (again, for both NSTAP and Pitot tube datasets). In Figure 5, the relative differences  $\epsilon_{u_\tau}$  between these different friction velocity estimates scaled with the Fernholz correlation estimate are presented for all cases, where  $\epsilon_{u_\tau} = (u_{\tau C} - u_{\tau F})/u_{\tau F}$ . As can be seen, most of the estimates lie within  $\pm 5\%$  except for the lowest Reynolds number case, probably because the log law applies only over a very limited range of wall distances at this Reynolds number. In light of this level of agreement among the different estimates of  $u_\tau$ , the value from the Fernholz correlation is used for all subsequent data analysis.

The mean velocity profiles from the NSTAP and Pitot measurements are compared in Figure 6 in inner variables. Good collapse of the profiles can be seen from the linear region at the wall (where  $y^+ = U^+$ , shown as a solid line for reference) throughout the near-wall region. The logarithmic region is evident for all cases, though only for a very small region at the lowest Reynolds number. In order to better quantify the differences between the profiles,

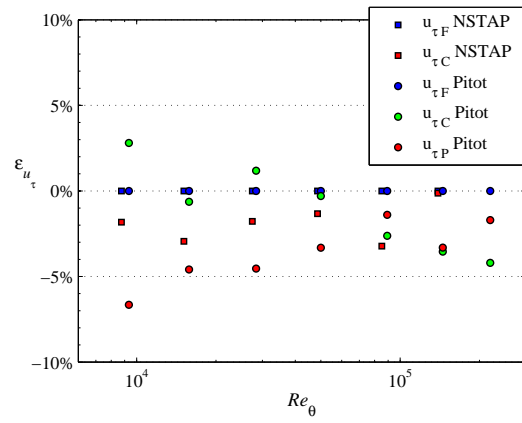


Figure 5. Difference between friction velocity estimates from Clauser fit and Preston tube measurements compared to the results from the Fernholz relation.

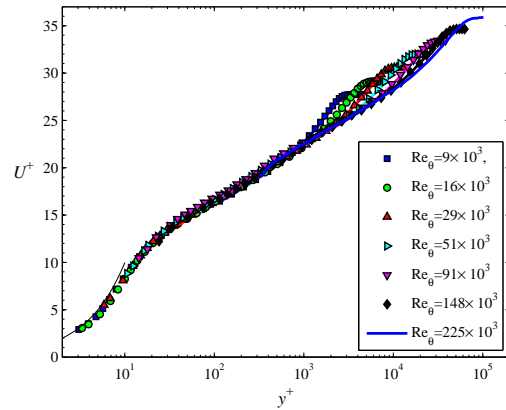


Figure 6. Mean velocity profiles measured with  $60\mu\text{m}$  NSTAP probe (symbols) and Pitot tube (lines). For  $Re_\theta = 225 \times 10^3$  only a Pitot probe profile is available. The viscous sublayer relationship  $U^+ = y^+$  is also shown for  $y^+ \leq 10$  as a solid line.

Figure 7 shows each profile shifted by a constant factor of  $\Delta U^+ = 5$ . The data show an excellent agreement between the profiles throughout the whole boundary layer.

Relative differences at every measurement point  $\epsilon_U$  were also estimated and the results are presented in Figure 8, where  $\epsilon_U = (U_{NSTAP}^+ - U_{Pitot}^+)/U_{NSTAP}^+$  and NSTAP results were used as a reference. The average relative error mostly varied between 0.2% and 0.8%, and the maximum error was less than 1% for most wall locations and Reynolds numbers, with only a couple of outliers. This agreement is well within experimental error, as the uncertainty in measurements of  $U$  under these experimental conditions is estimated to be as high as 2.2%.

Table 2 lists the boundary layer thickness  $\delta = \delta_{99}$ , as well as the momentum thickness  $\theta$ , the displacement thickness  $\delta^*$ , and the shape factor  $H = \delta^*/\theta$  for each case. Figures 9 and 10 show  $\theta$  and  $\delta^*$  scaled with  $\delta_{99}$ , and it can be seen that they both decrease with increasing  $Re_\theta$ , as expected. The shape factor also shows the expected

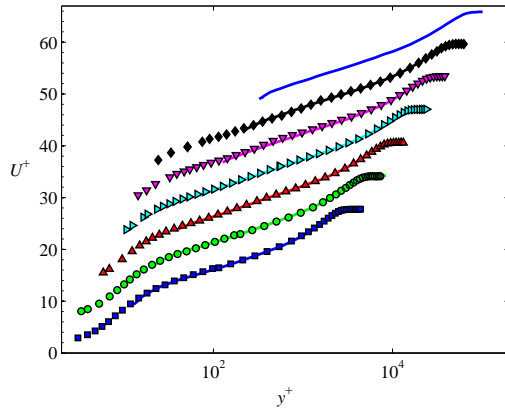


Figure 7. Mean velocity profiles measured with an NSTAP probe (symbols) and Pitot tube (lines), each shifted in  $U^+$  by  $\Delta U^+ = 5$ . Symbols same as in Figure 6.

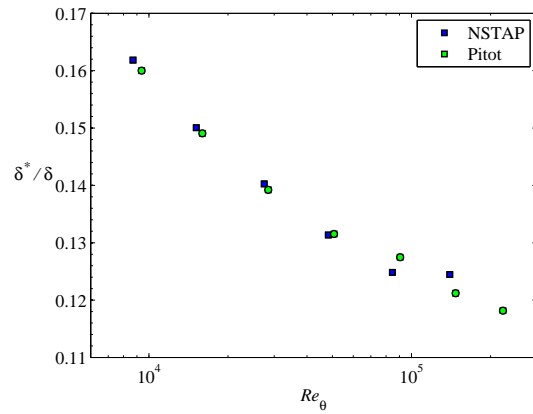


Figure 9. Displacement thickness  $\delta^*$  scaled with  $\delta$  as a function of Reynolds number  $Re_\theta$ .

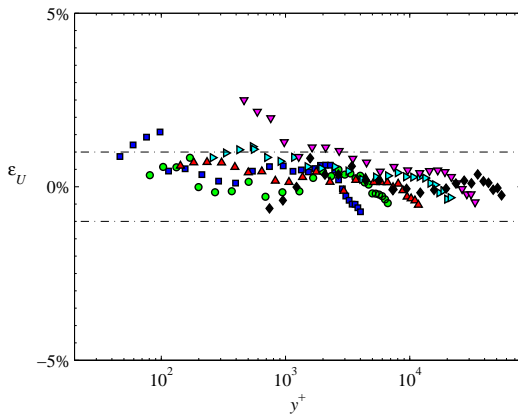


Figure 8. Relative errors between profiles measured with an NSTAP probe and a Pitot tube. Symbols same as in Figure 6.

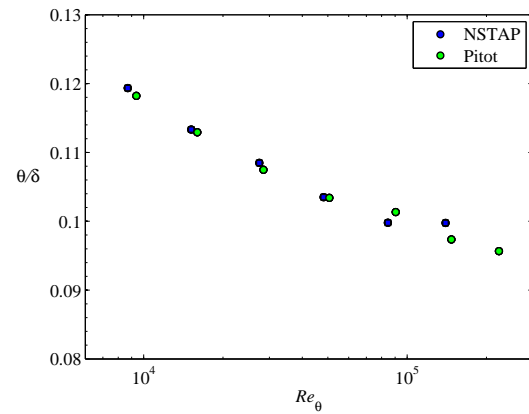


Figure 10. Momentum thickness  $\theta$  scaled with  $\delta$  as a function of Reynolds number  $Re_\theta$ .

trend of decreasing with increasing  $Re_\theta$ . The friction factor  $C_f = 2\tau_w / \rho U_c^2$  is also given in Table 2 and in Figure 11. Error bars corresponding to  $\pm 5\%$  are shown for the current experiment at the lowest and highest Reynolds number cases. The data are compared to the experimental results reported in DeGraaff & Eaton (2000), and the correlations suggested by Fernholz & Finley (1996), George & Castillo (1997), and Smits *et al.* (1983). Again, the data from Pitot and NSTAP agree very well, and they also agree with the experiments from DeGraaff & Eaton, within the uncertainty. The Fernholz relation was used to find  $u_\tau$  so it agrees with the data, by definition. The Smits *et al.* relation agrees with the data for  $Re_\theta < 5000$  (it was based on data for  $Re_\tau < 3000$ ) while George & Castillo's relation is in better agreement at higher Reynolds numbers.

The von Kármán constant  $\kappa$  for every profile was estimated in the region between  $y^+ > 3Re_\tau^{0.5}$  and  $y/\delta < 0.15$ . The average over all cases gave  $\kappa = 0.394 \pm 0.015$ . Giving an estimate within 4% is a reasonable scatter bearing in mind the experimental errors and that the friction velocity

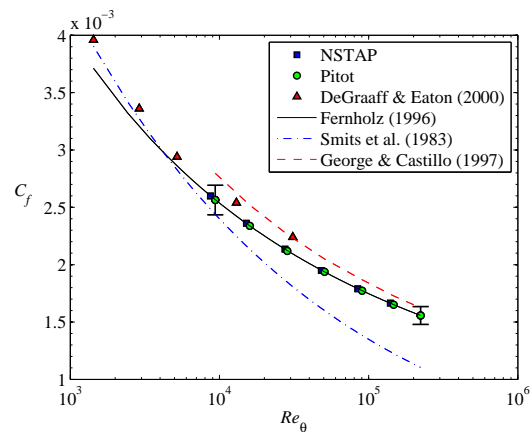


Figure 11. Friction factor  $C_f$ . The Fernholz correlation is from Fernholz & Finley (1996), and the power law correlation is from Smits *et al.* (1983).

August 28 - 30, 2013 Poitiers, France

Table 2. Bulk properties. Dimensional quantities in mm.

Case	$\delta$	$\delta^*$	$\theta$	$H$	$C_f \times 10^3$
1	27.5	4.45	3.29	1.35	2.60
2	27.7	4.15	3.13	1.32	2.36
3	28.3	3.97	3.07	1.29	2.14
4	27.3	3.59	2.83	1.27	1.95
5	26.4	3.3	2.64	1.25	1.79
6	25.9	3.22	2.58	1.25	1.66
7	28.7	4.59	3.39	1.35	2.56
8	28.6	4.26	3.23	1.32	2.34
9	29.1	4.06	3.13	1.29	2.12
10	28.1	3.69	2.90	1.27	1.94
11	27.0	3.44	2.73	1.26	1.77
12	26.5	3.21	2.58	1.24	1.65
13	25.7	3.04	2.46	1.23	1.56

was indirectly estimated using Fernholz & Finley (1996). The average additive constant over all profiles was found to be  $B = 4.7 \pm 0.83$  but it needs to be noted that this constant is very sensitive to the value of  $\kappa$  as well as  $u_\tau$  and the uncertainty in the wall-normal distance. These values agree well with the results from Marusic *et al.* (2013), who found  $\kappa = 0.39$  and  $B = 4.3$ . For consistency with this previous work, we will use the values from Marusic *et al.* (2013) for further analysis.

In order to estimate the extent of the logarithmic layer in the profiles we introduce the parameter  $\Phi$ , where

$$\Phi = U^+ - \frac{1}{\kappa} \ln y^+ - B. \quad (2)$$

In the region where the log law should apply, plotting  $\Phi$  against the wall-normal positions a horizontal line should be evident, assuming that  $\kappa$  was chosen correctly. In Figures 12 and 13 this function is shown in inner and outer wall coordinates, respectively, with straight lines indicating the respective zero values for each Reynolds number. From Figure 13 it is clear that the outer limit of the logarithmic layer agrees well with  $y/\delta = 0.15$ , which is also indicated on the plots with the error bar locations.

Determining the inner limit for logarithmic behavior is less clear, as no obvious departure from logarithmic region can be seen. It can be seen that all profiles are slightly curved near the wall, which could indicate the presence of a mesolayer with a power law like behavior as found in pipe flow by McKeon *et al.* (2004). The lower limit of  $y^+ > 3Re_\tau^{0.5}$  suggested by Marusic *et al.* (2013) is denoted with error bars in Figure 12, and this limit is in reasonable agreement with the data, although we can make no final conclusions on the inner limit of the logarithmic layer due to the uncertainties in the measurements near the wall.

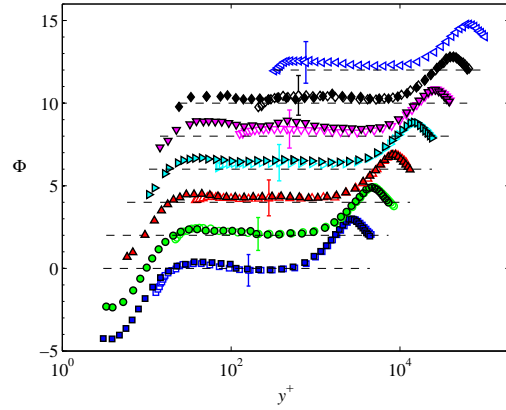


Figure 12. Mean velocity profiles with log function in inner coordinates. Profiles have been shifted in  $\Phi$  for clarity. NSTAP probe (filled symbols) and Pitot tube (empty symbols), otherwise symbols same as in Figure 6.

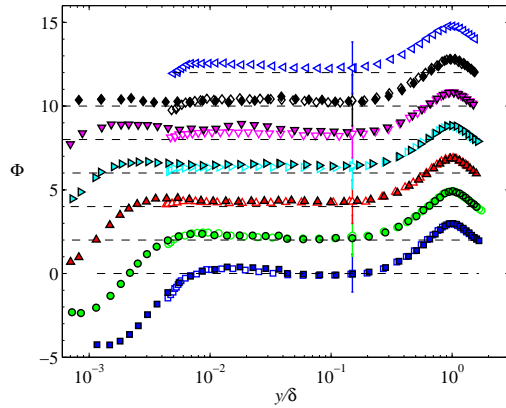


Figure 13. Mean velocity profiles with log function in outer coordinates. Profiles have been shifted in  $\Phi$  for clarity. NSTAP probe (filled symbols) and Pitot tube (empty symbols), otherwise symbols same as in Figure 6.

## CONCLUSIONS

Measurements over a wide range of Reynolds numbers have been performed in a turbulent zero pressure gradient boundary layer using novel NSTAP probes, as well as with conventional Pitot tubes. The Reynolds numbers spanned the range  $8.8 \times 10^3 \leq Re_\theta \leq 225 \times 10^3$ , corresponding to  $2.6 \times 10^3 \leq Re_\tau \leq 66 \times 10^3$ . Several indirect methods were used to estimate the skin friction coefficient, and it was shown that these estimates agreed within  $\pm 5\%$ . Mean velocity measurements from NSTAP and Pitot techniques have been compared and a very high level of agreement between both methods was demonstrated. The extent and validity of the logarithmic region was estimated and it was found that the current data agree well with Marusic *et al.* (2013), who find  $\kappa = 0.39$  and  $B = 4.3$  for a log law extending from  $y^+ = 3Re_\tau^{0.5}$  to  $y/\delta = 0.15$ .

This work was made possible by support received

through ONR Grant N00014-09-1-0263, program manager Ronald Joslin, and NSF Grant CBET-1064257, program manager Henning Winter.

## REFERENCES

- Bailey, S. C. C., Kunkel, G. J., Hultmark, M., Vallikivi, M., Hill, J. P., Meyer, K. A., Tsay, C., Arnold, C. B. & Smits, A. J. 2010 Turbulence measurements using a nanoscale thermal anemometry probe. *J. Fluid Mech.* **663**, 160–179.
- Clauser, F. H. 1956 The turbulent boundary layer. *Advances in Mechanics* **4**, 1–51.
- DeGraaff, D. B. & Eaton, J. K. 2000 Reynolds-number scaling of the flat-plate turbulent boundary layer. *J. Fluid Mech.* **422**, 319–346.
- Fernholz, H. H. & Finley, P. J. 1996 The incompressible zero-pressure-gradient turbulent boundary layer: an assessment of the data. *Prog. Aerospace Sci.* **32**, 245–311.
- George, W. K. & Castillo, L. 1997 Zero-pressure-gradient turbulent boundary layer. *Appl. Mech. Rev.*, **50**, 689–729.
- Hultmark, M., Vallikivi, M. & Smits, A. J. 2012 Turbulence at extreme Reynolds numbers. *Phys. Rev. Lett.* **108**, doi: 10.1103/PhysRevLett.108.094501.
- Jiménez, J. M., Hultmark, M. & Smits, A. J. 2010 The intermediate wake of a body of revolution at high Reynolds number. *J. Fluid Mech.* **659**, 516539.
- M. V. Zagarola, D. R. Williams & Smits, A. J. 2001 Calibration of the preston probe for high reynolds number flows. *Meas. Sci. Technol.* **12**, 495501.
- MacMillan, F. A. 1956 Experiments on Pitot-tubes in shear flow. *Tech. Rep.*. Aero. Res. Council.
- Marusic I., McKeon, B. J., Monkewitz, P. A., Nagib, H. M., Smits, A. J. and Sreenivasan, K. R. 2010 Wall-bounded turbulent flows: recent advances and key issues, *Phys. Fluids*, **22**, 065103.
- Marusic, I., Monty, J., Hultmark, M. & Smits, A. J. 2013 On the logarithmic region in wall turbulence. *J. Fluid Mech.* **716**, R3.
- McKeon, B. J., Li, J., Jiang, W., Morrison, J. F. & Smits, A. J. 2003 Pitot probe corrections in fully developed turbulent pipe flow. *Meas. Sci. Tech.* **14** (8), 1449–1458.
- McKeon, B. J., Li, J., Jiang, W., Morrison, J. F. & Smits, A. J. 2004 Further observations on the mean velocity distribution in fully developed pipe flow. *J. Fluid Mech.* **501**, 135–147.
- Nagib, H. M. & Chauhan, K. A. 2008 Variations of von Kármán coefficient in canonical flows. *Phys. Fluids* **20**, 101518.
- Österlund, J. M., Johansson, A. V., Nagib, H. M. & Hites, M. H. 2000 A note on the overlap region in turbulent boundary layers. *Phys. Fluids* **12** (1), 1–4.
- Patel, V. C. 1965 Calibration of the Preston tube and limitations on its use in pressure gradients. *J. Fluid Mech.* **23**, 185–208.
- Smits, A. J. and Matheson, N. and Joubert, P. N. 1983 Low Reynolds number turbulent boundary layers in zero and favourable pressure gradients. *J. Ship Res.*, **27**, 147–157.
- Smits, A. J. and McKeon, B. J. and Marusic, I. 2011 High Reynolds number wall turbulence, *Annu. Rev. Fluid Mech.*, **43**, 353–375.
- Vallikivi, M., Hultmark, M., Bailey, S. C. C. & Smits, A. J. 2011 Turbulence measurements in pipe flow using a nano-scale thermal anemometry probe. *Expts. Fluids* **51**, 1521–1527.
- Zagarola, M. V. & Smits, A. J. 1998 Mean-flow scaling of turbulent pipe flow. *J. Fluid Mech.* **373**, 33–79.